1.4 CHARCTERISTICS ANALYSIS AND INFLUENCE OF ENVIRONMENTAL VARIABILITY ON IDEALIZED SIMULATIONS FOR A LONG-LIVED BOW ECHO WITH HIGH PRECENTAGE OF POSITIVE CLOUD-TO-GROUND LIGHTNING

DAI Jianhua*, TAO Lan, SUN Min
Shanghai Central Meteorological Observatory, Shanghai, China
YUAN Zhaohong
Shanghai Meteorological Service, Shanghai, China

1. INTRODUCTION

On 5 June 2009, there was a high level cold vortex that was abnormally strong and stable during the month of June over the Northeast China (Fig. 1). Central of the east China region was behind a aloft trough. High level jets at the south-west part of the vortex brought strong cold advection that lowered down the freezing level and increased lapse rate (instability) and vertical wind shear. It is one of five synoptic conceptual models of severe convection in this region, with a dry and unstable environment (Sun et al., 2014).

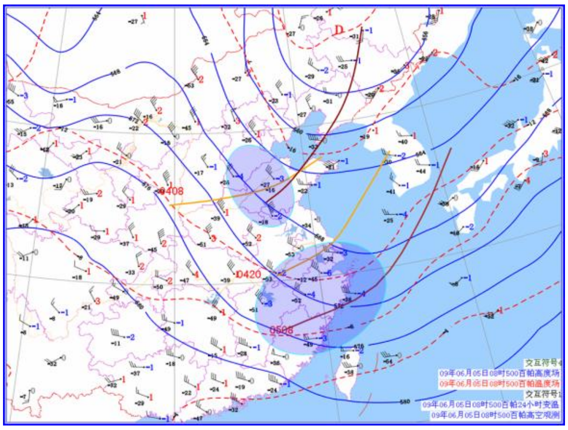

Fig. 1 Synoptic analysis of 08:00(BJT) 500 hPa (trough with brown, previous trough with orange, and temperature change in last 24 hours with shaded sky-blue) on Jun 5, 2009. (Soundings: XZ-Xuzhou, BS-Baoshan)

A Mesoscale Convective System (MCS) was triggered just underneath the high-level north-westerly jets and along low-level convergence line in the central Jiangsu Province (Fig. 2). It lasted for about 10 hours with a bow echo during its mature stage. The MCS brought widely large hail stones and strong straight-line winds for Jiangsu Province, Shanghai, and Zhejiang Province in the East China region. Several studies (Yin et al., 2010; Dai et al., 2012) have focused on this MCS and a supercell ahead of the MCS.

The MCS was dominated by positive could-to-ground (CG) lightning flashes (percentage over 66%) rather than negative CG lightning flashes at the early stages, which was much higher than most of other MCSs (MacGorman et al., 1989; MacGorman and Nielsen, 1991; Makowski et al., 2013).

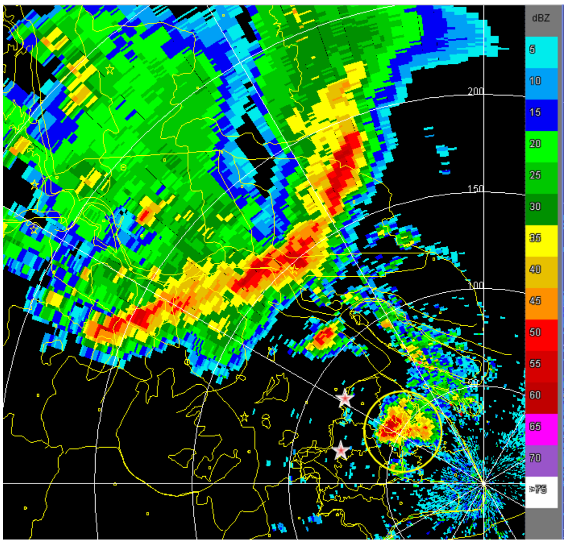

Fig. 2 Base reflectivity (in dBZ) from the 0.5° scan of the Shanghai WSR-88D, 07:04Z June 5, 2009.

CG lightning flashes were observed in MCSs or severe thunderstorms and studied by many studies (Rust et al., 1981; MacGroman, 1988; Rutledge and MacGorman, 1988; Reap and MacGroman, 1989; Williams et al., 1989; Engholm et al. 1990; Saunders et al., 1991; Knapp, 1994; Parker and Johnson, 2001). At the same time, many studies have focused on positive CGs (Rust et al. 1981; MacGroman 1988; Engholm et al. 1990; Saunders et al., 1991; Morrison et al., 2009). Many positive flashes discharge at upper levels in the anvil severe storms by the advection of positive charge from the major convection regions or at those area adjacent to convective storms which are associated with a local tilted electrical dipole. In the stratiform precipitation regions of MCSs, some positive flashes are caused by the advection of positive charge from the upper levels of the convective portions of the storm. However, an additional class of positive ground flashes are associated with the generation of charge by stratiform precipitation processes, specifically related to ice-ice interactions in regions of low supercooled liquid water contents. In some severe thunderstorms, an inverted-polarity structure is found with positive graupel charging occurs at temperatures above a "charge sign reversal temperature" , and the reversal temperature moves to lower temperatures when the liquid water content is increased.

* *Corresponding author address:* Jianhua Dai, Shanghai Central Meteorological Observatory, Shanghai 200030, China; e-mail: djhnn@sina.com.

Some MCSs were found with a bow-shaped echo and long-lived (Bluestein and Jain, 1985; John and Hirt, 1987; Przybylinski R W. 1995). In this study, the horizontal and vertical structure of the bow echo is analyzed using weather Doppler radars. The reasons of dominant CG polarity change during this squall line's evolution are discussed. In order to investigate the environmental influence on the development and evolution of this squall line, idealized simulations using a WRF meso-scale numerical weather prediction (NWP) model are made (Yuan, 2015; NCAR), according to five schemes by modifying the near-storm environmental sounding data.

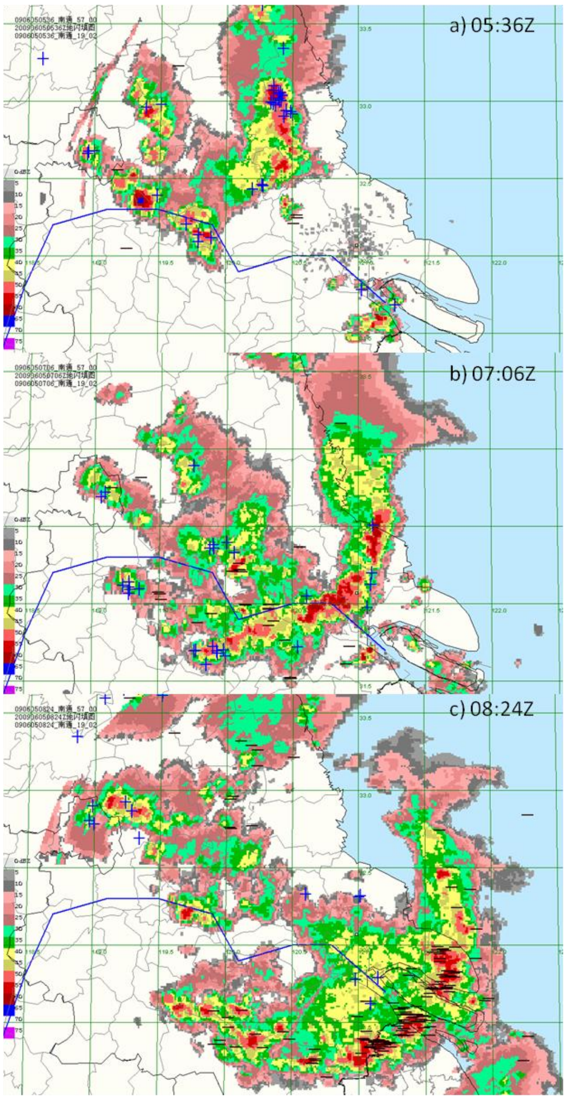

Fig. 3 Nantong Doppler radar's reflectivity (dBZ) and 6-min ADTD CG lightning flashes (blue + denotes for positive, and black - for negative) at a) 05:36Z, b) 07:06Z, and c)08:24Z, June 5, 2009

2. EVOLUTION OF THE MCS

2.1 Formation and Development

Some thunderstorm cells initiated in the central Jiangsu Province at noon and started to merger together as a MCS at about 14:00 (06:00Z). After formation, the area the MCS was increasing significantly. Then, the MCS gradually developed as a bow echo after passing through the Yangtze River (Fig. 3). This MCS also showed some characteristics of a squall line on radar images, such as a MARC (mid-altitude radial convergence) and a RIJ (rear inflow jet) (Fuquay 1982; Weisman 1982; Smull and Houze, 1987).

2.2 CG Lightning Activity

During the formation and development of the MCS, cloud-to-ground lightning activity was detected by the China Meteorological Administration (CMA) lightning detection network (ADTD). Positive CG lightning dominated in its early stages (Fig. 3a and Fig. 3b), while after it organized well negative CG lightning burst out (Fig. 3c). Positive flashes were found associated with the strong cells of the MCS in the early stages, which reveals that an inverted-polarity structure with positive graupel charging might occur at temperatures above a 'charge sign reversal temperature' (Saunders et al., 1991). When negative flashes burst out along the major part of the bow echo, few positive flashes only were found at stratifrom regions of the MCS indicating that positive ground flashes were caused by the advection of positive charge from the major convective region (MacGroman 1988; Engholm et al. 1990).

2.3 Reason Analysis of High Positive CG Ratio

Radar reflectivity cross section with heights of the freezing level and -20 ℃ are compared to investigate the vertical structure of the MCS and the possible micro-physics processes and charging mechanisms. PPCG (Percentage of Positive CG lightning) is also calculated.

During the early stages of the MCS lifecycle, several strong storms with some supercell signs (e.g., meso-cyclone and weak echo region) developed and merged together, with surface reports of hails and downbursts. Cross sections show the strong reflectivity cores were above -20℃ level with high possibility of large hail (Fig 4a). Nearly 80% of CG lightning flashes were positive.

Half and an hour later, MCS's size enlarged and its PPCG was still in the high level over 60% (Fig 4b). The cell at south-west part of MCS was the highest and strongest. Some negative CG flashes were found at the north-east part of the MCS where storms were weakening. At 07:05Z (Figure not shown) , the major part of MCS developed as a bow echo with high positive CG ratio. After that, the PPCG started to go down from 60% as more negative CGs observed just behind the major convective line.

At 07:29Z (Fig. 4c), along the well-developed bow echo, the elevated strong reflectivity had been descending. Strong straight winds were found at the area bow echo passing. Many negative CGs were detected along the bow echo. The PPCG dropped dramatically down to below 20% and most of positive flashes were found in the stratifrom regions or new cells.

Around 08:00 UTC (Fig. 4d), the vertical cores of the most of cells along the bow echo fell down below the -20℃ level and negative CGs dominated with a PPCG below 10%. At the same time, however, there were some tall cells developing with strong reflectivity over 55dBZ above the -20℃ level at the southwest end of the MCS. After that, positive flashes were detected in new cells the south-west part.

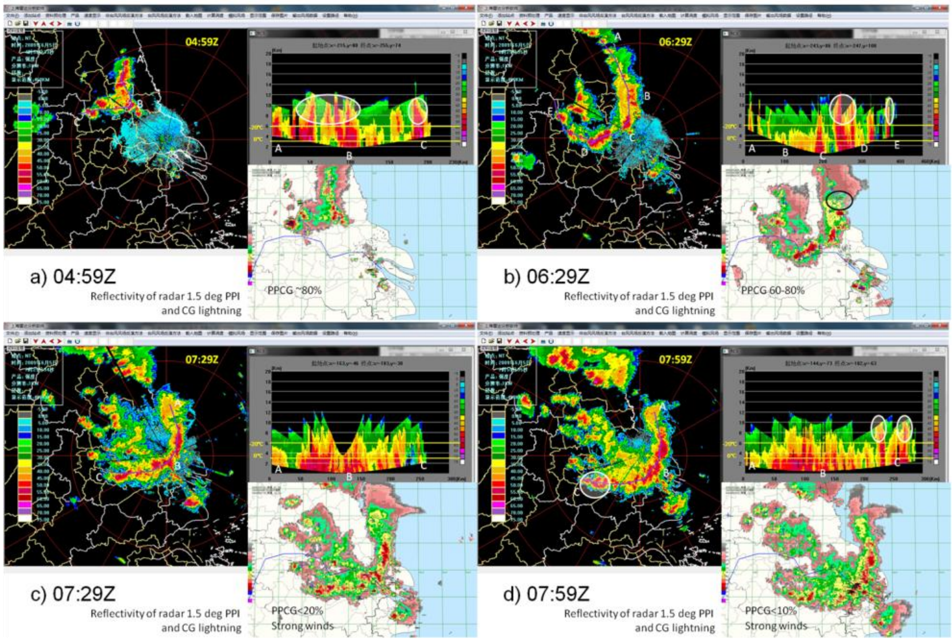

Fig. 4 Nantong PPI and cross section display of reflectivity (dBZ) with heights of the freezing level and -20 ℃, and 6-min ADTD CG lightning flashes (blue + denotes for positive, and black - for negative) at a) 04:59Z, b) 06:29Z, c) 07:29Z, and d) 07:59Z, on June 5, 2009

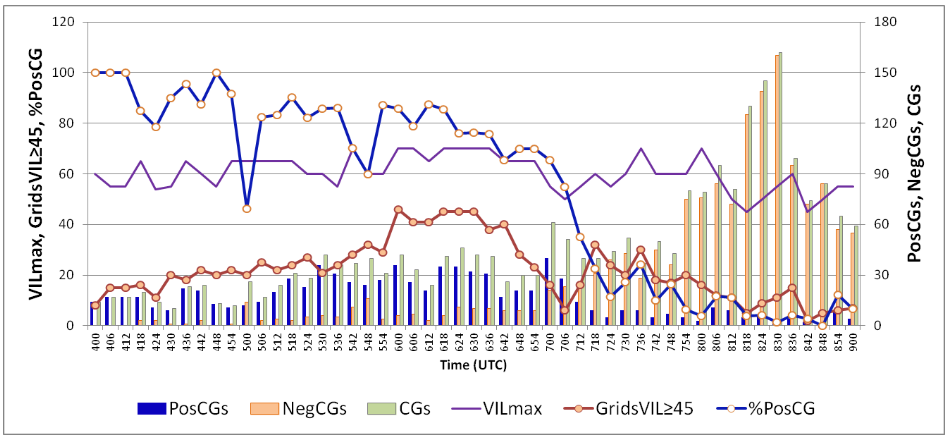

Fig. 5 Time series of 6-min (1) Nantong Doppler radar's VIL maximum (VILmax - kg/m^2, purple line) and Grids of VIL ≥ 45 kg/m^2 (GridsVIL, light brown line), (2) the ADTD +CG lightning proportion (%PosCG - %, blue line), +CG lightning flashes (CGs, flash, blue bars), -CG lightning flashes (NegCGs, flash, green bars), and total CG lightning flashes (flash, light orange bars) , 0400-0900 Z, June 5, 2009

Fig. 5 shows time series of 6-min the maximum Vertically Integrated Liquid (VIL), the area of VIL exceeding 45 kg/m^2, and positive, negative, and total CG lightning flashes and PPCG. The PPCG was over 60% in the early stages and dropped rapidly after 07:00Z down to 5% at 08:00Z. The area of VIL of MCS above 45 kg/m^2 peaked 30-60 min before the lightning polarity suddenly changed.

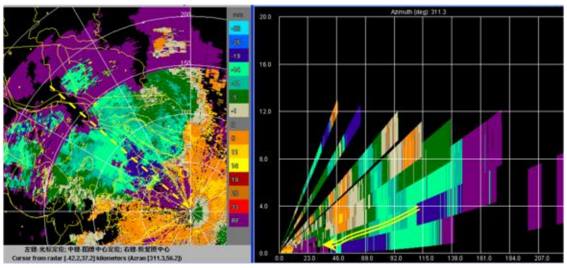

Fig. 6 Base radial velocity (left) and vertical cross section of velcoity (right) along the yellow dotted line at left panel at 08:36Z show a descending rear to front inflow jet

Fig. 6 shows a descending rear inflow jet of the MCS when low level vertical wind shear and was not strong enough to elevated it.

The cross sections of the Dual-Doppler radar retrieval winds (Fig. 7) along the MCS's axis are shown for 0630Z and 07:30Z. When PPCG was as high as 70-90% at 0630Z updrafts dominated in the MCS, while PPCG started to drop when downdrafts started at 07:00Z (not shown). When the RIJ with the downdrafts reached surface, nearly 90% of CGs were negative at 07:30Z (Fig. 7).

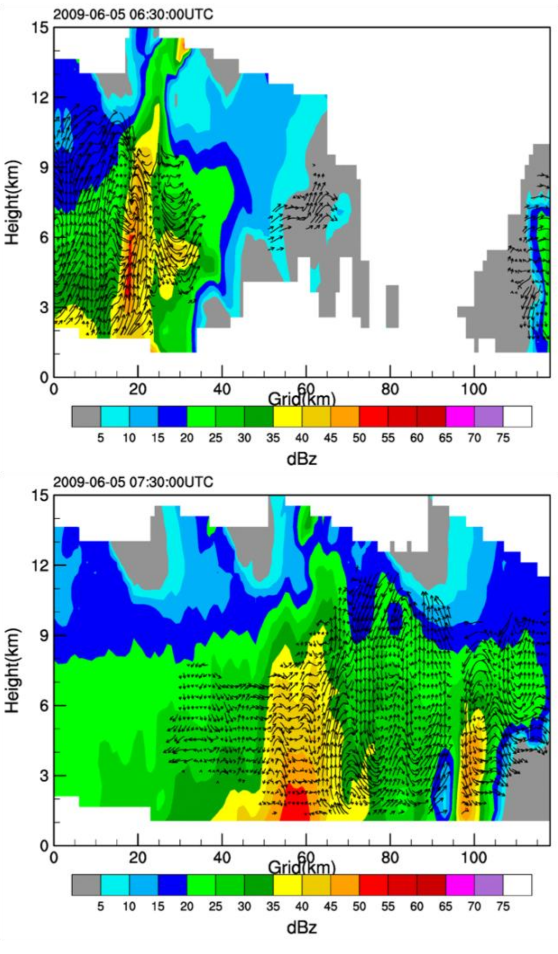

Fig. 7 Vertical cross sections of 06:30Z (upper) and 07:30Z (bottom) dual-Doppler radar wind retrievals.

3. NEAR-STORM ENVIRONMENT ANALYSES AND COMPARISONS

Environment factors are compared for the initiation phase and mature phase of the MCS using two radiosond stations: 1) the Xuzhou sounding station (XZ in Fig. 1) which was located at upstream of the MCS initiated; and 2) the Baoshan sounding station (BS in Fig. 1) which was close to where the bow echo formed with the burst of negative CG lightning flashes. The 00Z Xuzhou sounding is modified by changing surface temperature and dew-point using 06Z surface reports representing the environment of the initiation and evolution of the early stages of the MCS with a abnormally high positive CG lightning ratio. The 06Z Baoshan sounding released 2-hr prior to the MCS arrival can be used to represent the environment during the mature stages of MCS, especially for the period with a rapid change of predominated CG lightning polarity form positive to negative.

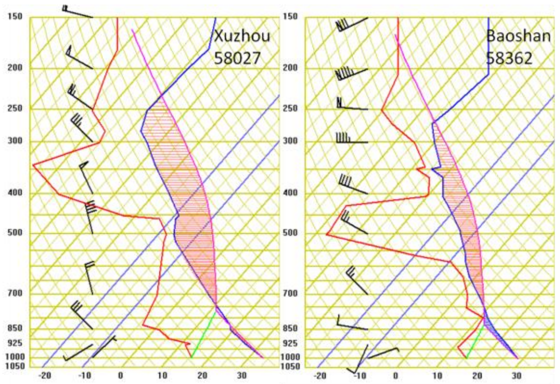

Fig. 8 Sounding comparisons between two stations: 1) 58027-Xuzhou (left) at 00Z modified by using 06Z surface temperature and dewpoint; 2) 58362-Baoshan at 06Z

Fig. 8 shows the comparisons between these two soundings. Both of these soundings have mid-convective available potential energy and weak-to-mid 0-6km wind shear relative to other strong and long-lived MCSs (Evans and Doswell, 2001; Coniglio et al., 2004; Cohen et al., 2007). The positive-CG cells occurred in the environment (Fig. 8 left panel) with dryer low levels, higher lifted condensation level (LCL), thinner warm cloud depth (WCD), larger instability (low-level lapse rate) and bigger 0-6km and 0-3km wind shears than those of the negative-CG predominated MCS (Fig. 8 right panel) (Williams et al. 2005; Carey and Buffalo 2007).

Some studies on lightning microphysics (Takahashi, 1978 ; Knapp ,1994; Williams et al., 2005; Carey and Buffalo, 2007) show that larger cloud water concentrations in the mixed phase region via the non-inductive charging (NIC) mechanism will be a favorable condition for the positive charging of large ice particles that may result in thunderclouds with a reversed polarity of the main cloud dipole. Graupel concentrations in the lower part of the updraft's mixed-phase region can gain a positive charge by noninductive charge exchange with cloud ice in a classical tripole charge distribution. This situation will be less relative to graupel concentrations in the updrafts of storms with a warmer cloud base. The lower positive charge carried by graupel would be similarly reduced.

Environment conditions for this situation are associated with an elevated cloud base height (CBH) (low sub-cloud moisture) and shallow warm-cloud depth (WCD). Broad and intense updrafts (CAPE - convective available potential energy at the levels between -10℃ and -40 ℃) and high liquid water contents (LWC) will keep less entrainment of ambient air and transport a larger fraction of water content to the mixed-phase region. As a conclusion, positive CG flashes were found under a drier low to mid-troposphere, higher cloud-base height, smaller warm cloud depth, stronger conditional instability, larger 0–3 km AGL wind shear, stronger 0–2 km AGL storm relative wind speed, and larger buoyancy in the mixed-phase zone (Carey and Buffalo, 2007).

4. IDEALIZED SIMULATIONS

In order to investigate environmental factors on influence of the MCS initiation and evolution as well as the high positive CG flash ratio in its early stages, idealized simulations using a WRF NWP model are made according to five schemes on modifying the convective parameters of the near-storm environmental sounding data, such as temperature lapse rate, low-level and mid-level humidity, and vertical wind shear (Yuan, 2015; NCAR).

4.1 Idealized Simulation Setup

The control run of the idealized simulation is based on the 06Z Baoshan sounding. Other five runs are setup by modifying some environmental factors. They are LLR (lower lapse rate), MML (moist mid-level), EMBL (extremely moist boundary layer), MBL (moist boundary layer), and LHLW (lower high-level winds). Detailed setup information of the five schemes are listed in Table 1).

Fig. 9b-9f show the idealized soundings compared to the control run (Fig. 9a). The environment shows a much higher LFC (level of free convection) and a smaller CAPE with a decreased lapse rate between 850hPa and 500hPa indicating mid-to-low level instability is crucial to thunderstorm initiation and development. The moist middle-level sounding (Fig. 9c) does not show any difference to most of convective indices, however, the convective instability is smaller due to the increase of moisture at mid-levels. When the moisture at boundary layer is increased, CAPE significantly increases and LFC lowers down (Fig. 9d and Fig. 9e).

4.2 Simulation Results

The simulation results, 2km-height reflectivity and wind vectors are shown in Fig. 10a-f. The control run (Fig. 10a) shows a bow echo which is similar to the observations (Fig. 2). Under an lower lapse rate environment, no convection is found in Fig. 10b. On moisture at mid-levels being increased, the horizontal size of MCS is smaller than that of the control run, which reveals that moist mid-levels will decrease the entrainment of mid-level dry air and diminish the evaporative cooling potential to lower downdrafts. As a feedback, the weakening interaction between the cool pool and ambient wind shear will make the size of MCS smaller.

Table 1. Idealized simulation schemes

ID.	Scheme	Sounding Modification
CTL	Control run	none
LLR	Lower lapse rate	decreased T850hPa and increased T500hPa and T300hPa
MML	Moist mid-level	increased dew point between 400 and 600 hPa
EMBL	Extremely moist boundary layer	dramatically increased dew point between surface and 925hPa (+8℃ and +6℃)
MBL	Moist boundary layer	increased dew point between surface and 925hPa (+5℃ and +3℃)
LHLW	Lower high-level winds	decreased wind speed between 300 and 500hPa

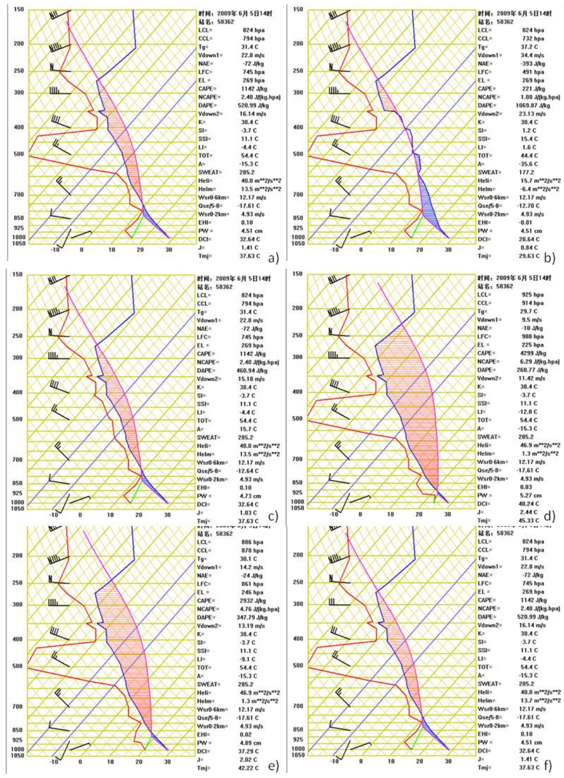

Fig. 9 Sounding analysis charts for the 06Z, a) control run, b) lower lapse rate, c) moist middle-level, d) extremely moist boundary, e) moist boundary, and f) lower high level winds of the 06Z Baoshan (ID:58362) sounding Shanghai, Jun. 5, 2009

When a extremely moist boundary layer meets, disorganized convection cells initiate dispersedly due to lack of convective inhibition (CIN) and very large convective available potential energy (Fig. 10d). If boundary layer moisture is increased properly, larger CAPE will transfer to strong updrafts to make the size of MCS larger and the downdrafts stronger than the control run (Fig. 10e).

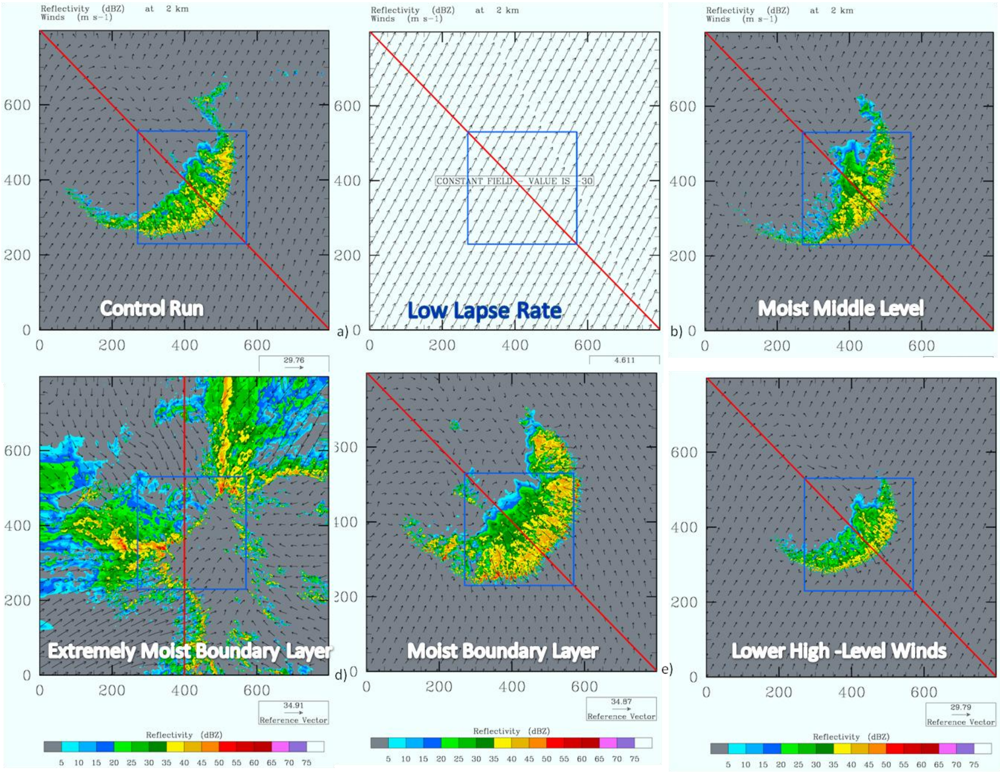

Fig. 10 the same as Fig. 9, except for reflectivity fields and wind vectors at the level of 2-km height by the WRF idealized simulations

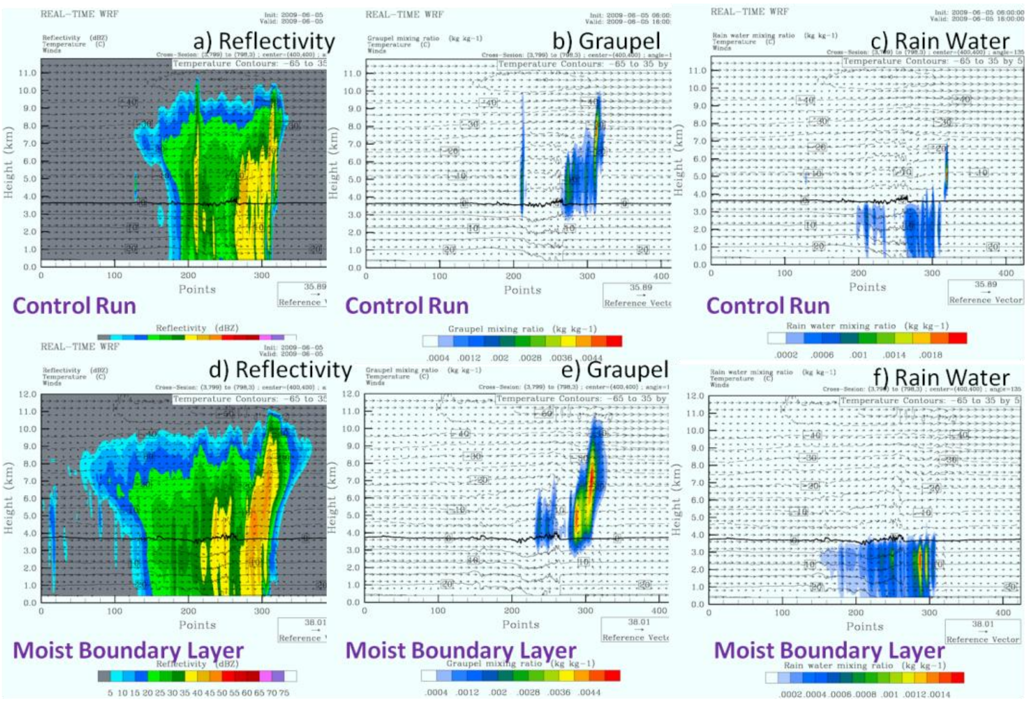

Fig. 11 Idealized model simulations of cross sections of wind vectors (m/s) with a) and d) reflectivity (dBZ), b) and d) graupel mixing ratio (kg/kg), and c) and f) rain water mixing ratio (kg/kg), along the axis of the MCS (the red line in Fig. 10) using the simulation schemes of a) to c) observed sounding data and d) to f) moist middle-level

When the surface to mid-level wind shear is lowered down by decreasing mid-level winds, the balance between cool pool and ambient wind shear is destroyed. As a result, new cells only initiate and develop close to the axis of the bow echo and the horizontal size of the MCS is much smaller than the others (Fig. 10f).

Fig. 11 compares two schemes of simulation, the control run and the moist boundary layer, using cross sections of graupel mixing ratio and rain water mixing ratio. Mosit boundary layer is found a larger warm cloud depth and lower cloud base height (Carey and Buffalo, 2007) and has much smaller probability of positive CG flash. When the MCS passed through the Yangtze river from dryer environment, the positive CGs predominated MCS transformed to a negative CGs predominated MCS due to a different lightning charging mechanism occurred in a new environment.

5. CONCLUSIONS AND DISCUSSIONS

A long-lived squall line with a bow echo occurred under a dry and unstable environment is analyzed using weather Doppler radars. The squall line showed some typical structural characteristics of bow echo, such as a mid-altitude radial convergence and a downward-sloping rear inflow jet. The bow echo was dominated by positive could-to-ground (CG) lightning flashes (percentage over 66%) rather than negative CG lightning flashes at the early stages. At its mature stage, burst of negative CG flashes were found in the major convection areas. The dominant positive CG lightning polarity was associated with rapid updraft intensification stages of the bow echo, and dominant negative CG with updraft weakening.

Idealized simulation results show: 1) the increasing lapse rate caused by the strong cold advection aloft over the warm advection at low levels was the crucial factor of a large convective energy or strong updrafts for this convection system. Warmer ambient air could enlarge the temperature difference between downdrafts and environment. 2) The rapid increase of boundary humidity was the major cause of this deep convection case by providing a lower LFC and a larger CAPE. 3) Dry layers at mid-levels and low-levels provided evaporative cooling potential to enlarge downdrafts (James et al., 2006).

The vertical and horizontal size of the MCS were sensitive to the strong vertical shear created by the high-level jets (based on model simulations). Along the squall line's motion axis, strong surface to high-level vertical wind shear interacted with the cold pool to enhance the lifting at the leading edge of the convective system, which made the squall line live longer (Thorpe et al., 1982; Weisman et al., 1988; Rotunno et al., 1988; Xue, 1990). On the other hand, The medium-to-weak vertical wind shear at low levels made a downward-sloping rear inflow jet which spread out along the surface and caused widely distributed strong wind gusts (Fuquay 1982; Weisman 1982).

Based model simulations and sounding comparisons, high cloud base and shallow warm-cloud layer can be the major cause of this high positive CG ratio MCS. The results are similar to other studies, such as, storms with a high cloud base and a resulting shallow layer for warm rain processes will shift precipitation growth to colder altitudes than found in storms with a warmer cloud base (Williams et al. 2005; Carey and Buffalo 2007). Future studies are planned to focus on micro-physics processes of high positive CG lightning flash ratio in a MCS.

6. REFERENCES

Bluestein H W and Jain M H. 1985: Formation of mesoscale lines of precipitation: Severe squall lines in Oklahoma during the spring. *J. Atmos. Sci*., 42: 1711–1732.

Carey, L. D., and K. M. Buffalo, 2007: Environmental control of cloud-to-ground lightning polarity in severe storms. *Mon. Wea. Rev.* 135, 1327-1353.

Cohen,A. E., M. C. Coniglio, S. F. Corfidi, and S. J. Corfidi, 2007: Discrimination of mesoscale convective system environments using sounding observations. *Wea. Forecasting*, 22:1045–1062.

Coniglio M C, Stensrud D J, and Richman M B. 2004: An observational study of derecho-producing convective systems. *Wea. Forecasting*, 19:320–337.

Dai, J., L. Tao, Y. Ding, et al. 2012: Case analysis of a large hail-producing severe supercell ahead of a squall line (in Chinese). *Acta Meteor. Sinica,* 70(4):609-627.

Engholm, C D, E R Williams, and R M Dole, 1990: Meteorological and electrical conditions associated with positive cloud-to-ground lightning. Mon. Wea. Rev., 118,470-487.

Evans J S and Doswell C A III. 2001: Examination of derecho environments using proximity soundings. *Wea. Forecasting*,16:329–342.

Fovell R G and Ogura Y. 1989: Effects of vertical wind shear on numerically simulated multicell storm structure. *J. Atmos. Sci*., 46: 3144–3176.

Fuquay, D. M. 1982: Positive cloud-to-ground lightning in summer thunderstorms, *J. Geophys. Res.*, 87, 7131-7140.

James R P, Markowski P M, J. Fritsch M. 2006: Bow Echo Sensitivity to Ambient Moisture and Cold Pool Strength. *Mon. Wea. Rev*., 134:950–964.

Johns, RH and Hirt WD. 1987: Derechos: Widespread convectively induced windstorms. *Wea. Forecasting,* 2:32–49.

Knapp, D. I., 1994: Using cloud-to-ground lightning data to identify tornadic thunderstorm signatures and nowcast severe weather. Natl. Wea. Digest, 19, 35–42.

Makowski J A, D R MacGroman, M I Biggerstaff, and W H Beasly. 2013: Total lightning characteristics relative to radar and satellite observations of Oklahoma mesoscale convcetive systems. *Mon. Wea. Rev*., 141:1593-1611.

MacGorman, D. R., D. W. Burgess, V. Mazur, et al., 1989: Lightning rates relative to tornadic storm evolution on 22 May 1981. J. Atmos. Sci., 46, 221-250.

MacGorman, D. R., and K. E. Nielsen. 1991: Cloud-to-ground lightning in a tornadic storm on 8 May 1986, Mon. Wea. Rev., 119, 1557-1574.

Morrison H, Thompson G, and Tatarskii V. 2009: Impact of cloud microphysics on the development of trailing stratiform precipitation in a simulated squall line: comparison of one- and two-moment cchemes. *Mon. Wea. Rev.*, 137:991-1007.

NCAR. User's Guide for the Advanced Research WRF (ARW) Modeling System Version 3.0., http://www.mmm.ucar.edu/wrf/users/docs/user_guide_V3.0/contents.html

Parker, M. D., S. A. Rutledge, and R. H. Johnson, 2001: Cloud-to-ground lightning in linear mesoscale convective systems. *Mon. Wea. Rev.*, 129, 1232–1242.

Przybylinski R W. 1995: The bow echo: Observations, numerical simulations, and severe weather detection methods. *Wea. Forecasting,* 10:203–218.

Reap, R. M., and D. M. MacGorman, 1989: Cloud-to-ground lightning: Climatological characteristics and relationships to model fields, radar observations and severe local storms, *Mon. Wea. Rev.*, 117, 518-535.

Rotunno R J, Klemp B, and Weisman M L. 1988: A theory for strong, long-lived squall lines. *J. Atmos. Sci.*, 45: 463–485.

Rust, W. D., D. R. MacGorman, and R. T. Arnold, 1981: Positive cloud-to-ground lightning flashes in severe storms, *Geophys. Res. Lett*., 8, 791-794.

Rutledge, S. A., and D. R. MacGorman,1988: Cloud-to-ground lightning activity in the 10-11 June 1985 mesoscale convective system observed during the Oklahoma-Kansas PRE- STORM Project, *Mon. Wea. Rev*., 116, 1393-1408.

Saunders C P R, Keith W D, and Mitzeva R P. 1991: The effect of liquid water on thunderstorm charging. *J. Geophys. Res.*, 96: 11007-11017.

Smull B F, and Houze R A. 1987: Rear inflow in squall lines with trailing stratiform precipitation. *Mon. Wea. Rev.*, 115:2869-2889.

Sun, J., J. Dai, L. He, et al., 2014: Methods and techniques for severe convection forecasting and nowcasting (the China Meteorological Administration forecasting handbook, in Chinese). *China Meteorological Press.*

Takahashi T. 1978: Riming electrification as a charge generation mechanism in thunderstorms, *J.* Atmos. Sci., 35: 1536-1548.

Thorpe A J, M J Miller, and M W Moncrieff. 1982: Two-dimensional convection in non-constant shear: A model of midlatitude squall lines. *Quart. J. Roy. Meteor. Soc.*, 108: 739-762.

Weisman M L, Klemp J B, and Rotunno R. 1988: Structure and evolution of numerically simulated squall lines. *J. Atmos. Sci.*, 45: 1990– 2013.

Weisman M L. 1992: The role of convectively generated rear-inflow jets in the evolution of long-lived mesoconvective systems. *J. Atmos. Sci.*, 49(19):1826–1847.

Williams E R, Weber M E, and Orville R E. 1989: The relationship between lightning type and convective state of thunderclouds. *J. Geophys. Res.,* 94:13213-13220.

Williams E R, V Mushtak, D Rosenfeld, S Goodman, and D Boccippio, 2005: Thermodynamics conditions favorable to superlative thunderstorm updraft, mixed phase microphysics and lightning flash rate. *Atmos. Res.,* **76,** 288–306.

Xue, M., 1990: Towards the environmental condition for long-lived squall lines: vorticity versus momentum. Preprints, *16th Conf. on Severe Local Storms*, Kananaskis Provincial Park, Alberta, Canada, Oct. 22-26, Amer. Meteor. Soc., 24-29.

Yin,D, H. Wu, B. Zhang, et al. 2010: Analysis on a severe convective weather triggered by sea breeze front (in Chinese). *Plateau Meteor*.,29(5):1261-1269.

Yuan,Z., 2015: Study of the influence of the different horizontal resolutions and microphysical setups on the idealized simulation of a squall line (in Chinese). *Acta Meteor. Sinica*, 73(4):648-666.